# Non-destructive testing derived parameters for microstructure-based residual service life assessment of aging metallic materials in nuclear engineering

Dedicated to Professor Dr. Dietmar Eifler on the occasion of his 70th birthday.

*Ruth Acosta, Christian Boller, Saarbrücken, Peter Starke, Kaiserslautern, Michael Jamrozy, Marina Knyazeva, Frank Walther, Dortmund, Klaus Heckmann, Jürgen Sievers, Cologne, Tim Schopf, and Stefan Weihe, Stuttgart, Germany*

***Article Information***

***Correspondence Address***
*MSc Ruth Acosta*
*Chair of Non-Destructive Testing and Quality Assurance*
*Saarland University*
*Am Markt Zeile 4*
*66125 Saarbrücken, Germany*
*E-mail: ruth.acosta@uni-saarland.de*

***Keywords***
*Nondestructive testing, fatigue life evaluation, fatigue, nuclear safety, material characterization, integrity assessment, AISI 347*

Metallic components in nuclear engineering are exposed to extensive loads such as pressurization and temperature changes which can affect the properties of the material significantly depending on the load spectrum applied. In view of developing a procedure to evaluate the residual service life of metallic components in nuclear power plants aged during service, metastable austenitic steel AISI 347 (German designation: X6CrNiNb18-10) has been considered as an example. To this purpose, total strain-controlled fatigue tests were carried out under different environmental conditions and monitored by continuously measuring thermometric, resistometric, electromagnetic and electrochemical parameters. These parameters provide an information gain in terms of material characterization when compared to conventional strain measurements. Based on these parameters, the short time evaluation procedure Strain-Life has been developed, which allows the determination of local S-N curves with a significantly reduced effort as compared with traditional procedures. This method has been implemented into the structural simulation program PROST for the integrity assessment of the components while considering local fatigue properties. This very effective method allows for the determination of local fatigue properties including the strain-specific local scatter of the metallic microstructure properties of the material which has not been possible by traditional means.

The reactor accident of Fukushima in 2011 led to a worldwide review of design principles and safety requirements of nuclear power plants, also taking the entire infrastructure required for a power plant's operation into account. This particularly concerned a consideration of accident scenarios occurring beyond a plant's design. The politically initiated so-called 'Energiewende' in Germany as a result of events in Fukushima is striving for a transformation from nuclear to renewable energy generation, and the review of safety standards has led to a large number of changes in the operation of nuclear power plants. This re-

quires increased attention with regard to the technical safeguarding of the operation of German nuclear power plants during their residual operational life. According to a report published in March 2013 by the Nuclear Technology Competence Alliance [1], there is an increased need for testing and evaluation regarding the safety and integrity of structures and components, which is primarily associated with methods related to the characterization of the materials and non-destructive testing (NDT) [2], as well as structure-mechanics analysis [3, 4].

The aim of the collaborative research project entitled 'Microstructure-based determination of the maximum service life for corrosion fatigue loaded materials and components of the nuclear technology' (MibaLeb) is to develop a procedure for the evaluation of the residual service life of nuclear power plant metallic components that have aged during operation. This project has been motivated by the fact that local material properties of such components can change significantly after prolonged operation and applies in particular when corrosive effects are added to the effects of mechanical and thermal stress.

## Material

**Initial state.** The material under investigation is niobium stabilized austenitic stainless steel AISI 347 which was delivered as round bars with a diameter of 30 mm and a length of 5,000 mm. The chemical composition according to the manufacturer's report is shown in Table 1.

Results of microstructural investigations on those bars showed that the material had significant inhomogeneity along the cross section in the initial state. This is presented in Figure 1a, where an image taken with a light microscope is displayed. The cross section of a bar was etched with V2A etchant, and a square-shaped zone was recognized macroscopically. Outside this area towards the sample edge, a strongly deformed and fine-grained austenitic structure is present, while inside, within the above-mentioned squared zone, a strongly inhomogeneous multiphase structure can be recognized. Moreover, electron back scatter diffraction (EBSD) measurements were used. From the analysis of the crystallographic information also shown in Figure 1b, mechanical twins and martensitic regions were observed in the coarser grained austenite structure at the center of the cross-section. The microstructure contains deformation induced α-martensite, formed during the manufacturing process of the bars. Twinning induced plasticity (TWIP) and transformation induced plasticity (TRIP) mechanisms present in the microstructure indicate low forming temperatures in the middle of the sample and a forming process through superficial heat input at the outer edge of the sample, respectively. The analysis of the magnetic permeability in terms of the ferromagnetic portion by means of a feritscope confirmed these metallographic results. The portion of ferromagnetic phase increases from the edge of the sample to the center of the cross-section, where it achieves its maximum of 0.8 % by volume which is attributed to the α-martensite ferromagnetic phase present at the center; ε-martensite could not be detected within these investigations.

The hardness curve along the cross-section presented in Figure 1c shows that the Vickers hardness is approximately 150 HV10 at the center of the cross-section and increases to approximately 170 HV10 towards the outer edge, which can be explained by the finer grain structure at the outer edge.

**Artificial aging.** The steel AISI 347 (X6CrNiNb18-10) exhibits a complex mechanical material behavior which is strongly dependent on the load level, deformation rate and service temperature [5]. For a detailed qualification of the non-destructive measuring methods developed and applied within the scope of the MibaLeb collaborative project, samples in the initial state, as well as samples in a defined aging condition were investigated. With respect to artificial aging, samples in the initial state were exposed to mechanical and thermal loads relevant in service. For applications in nuclear engineering, relevant loads are in the low cycle fatigue (LCF) range [6] superimposed by temperatures between T = 150 °C and 325 °C [7]. For this reason, the artificial aging of the samples was performed applying cyclic loading in air at a temperature of T = 240 °C, representing the average value of the above-mentioned temperature range, a total strain amplitude of $\varepsilon_{a,t} = 3 \times 10^{-3}$ and a strain rate of $\dot{\varepsilon}_{a,t} = 4 \times 10^{-3} s^{-1}$.

In view of determining the number of cycles to be used for the aging process, a database representing the initial condition of

| C | Cr | Ni | Mn | Si | Nb | P | Co | S | Fe |
|---|---|---|---|---|---|---|---|---|---|
| 0.025 | 18.147 | 10.064 | 0.577 | 0.401 | 0.402 | 0.024 | 0.019 | 0.0011 | bal. |

*Table 1: Chemical composition of AISI 347 (X6CrNiNb18-10) stainless steel according to manufacturer's report (wt.-%)*

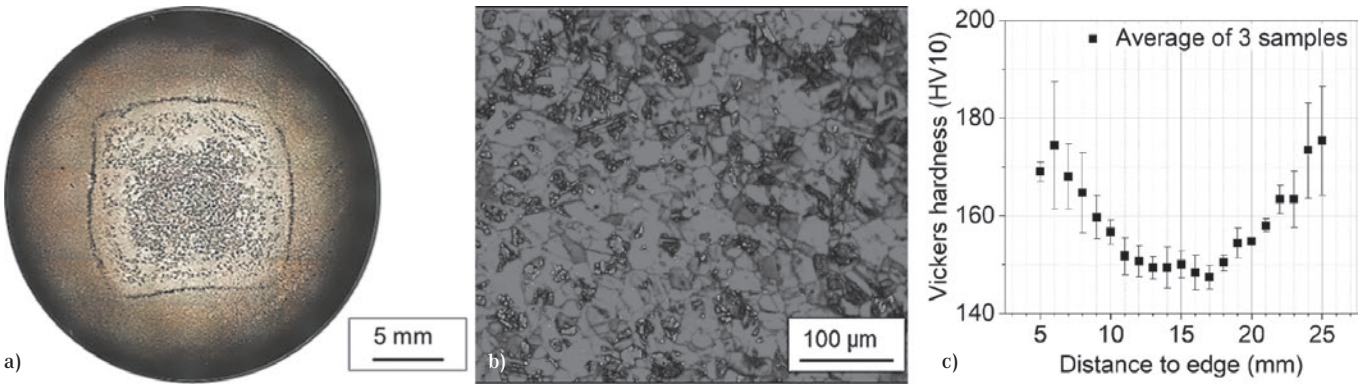


*Figure 1: Metallographic investigations of the cross-section of a sample, a) light microscopic image, b) EBSD phase distribution at the center of the cross-section: car grating (austenite), crisscross grating (martensite), c) Vickers hardness along the cross-section of the sample of AISI 347 (X6CrNiNb18-10)*

the material was generated, pre-treating four specimens under the above mentioned mechanical and thermal parameters and subjecting them to cyclic loading up to a defined failure criterion which in this case was a drop of 25 % in the stress amplitude. The lifetimes determined in terms of S-N data were evaluated by using statistical methods, whereby the number of cycles to failure for different survival probabilities (Ps) was calculated. This resulted in a number of cycles of 31,450 ($N_{25\,\%}$) for the evaluated tests at Ps = 95 %. The aging condition was defined as $0.5 \times N_{25\,\%}$ (Ps = 95 %), which resulted in 15,725 cycles for the mechanical pre-damage within the aging procedure. This ensures that the mechanical and thermal loads already cause the material to change from its original state to a significantly damaged state, without any macroscopically detectable damage characteristics. The probability, as well as the function of distribution, is shown in Figure 2. In addition to this, it also shows a comparison of tests of the same material but in another microstructural condition due to heat treatment, which is indicated as 'MPA database'.

## Experimental setup

Constant amplitude tests (CAT) and strain increase tests (SIT) were performed within the framework of the MibaLeb project. All tests were carried out with alternating total strains at a strain ratio of R = −1 and a constant total strain rate of $\dot{\varepsilon}_{a,t} = 4 \times 10^{-3} s^{-1}$, which was applied by means of a triangular strain-time function. The specification of the constant total strain rate results in different test frequencies f depending on the total strain amplitudes $\varepsilon_{a,t}$, which must be considered in both the SITs and the CATs.

The investigations were carried out under various environmental conditions, requiring three different testing setups, as shown in Figure 3. An instrumented specimen for experiments conducted at room temperature (RT) in air is shown in Figure 3a. The test setup includes an extensometer for controlling $\varepsilon_{a,t}$ during the experiment with a gauge length of 89 mm attached to the specimen shafts. Due to the need to implement additional measurement techniques as well as media chambers, it was not possible to use a conventional extensometer setup within the gauge length of the specimen for measurement and control. With respect to technical realization, the 89 mm extensometer was calibrated in preliminary tests by using an extensometer of 8 mm applied to the gauge length of the specimen, whereby a so-called correlated total strain amplitude $\varepsilon_{a,t,cor}$ was determined, which is an integral strain over the elastic-plastic deformed gauge length as well as the elastically deformed shafts. This procedure is particularly important in tests under medium conditions but also allows additional measurement technology to be placed onto the specimen's minimum cross-section when testing in air.

The various measurement techniques applied in tests at RT and in air include a feritscope [8], which is used to determine the ferromagnetic phase fractions due to deformation-induced martensite formation, as well as a self-developed magnetic field sensor consisting of a Hall sensor encapsulated via epoxy resin under vacuum inside a PTFE housing, arranged in the probe in such a way that it can detect the change in the tangential magnetic field on the surface of the specimen and in the surface near area. For magnetization, a constant direct current of I = 10 A was applied to the specimen. This sensor is used to detect changes in the magnetic field resulting from the martensitic phase transformation as well as microstructural changes due to dislocation reactions as well as crack formation and propagation at different scales.

As a further additional measurement variable, the change in electrical resistance [9] was recorded during the tests by meas-

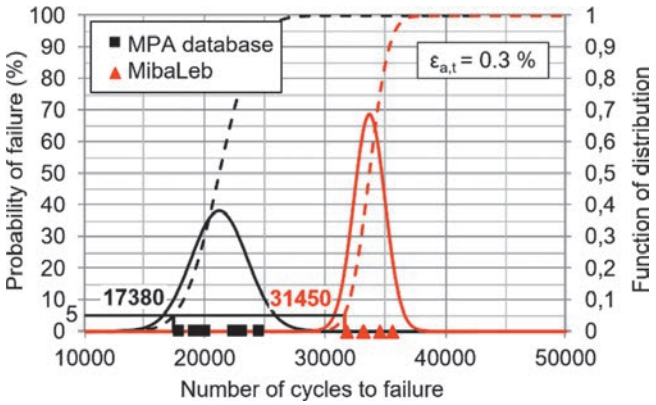


*Figure 2: Failure probability as well as the function of distribution for AISI 347 (X6CrNiNb18-10)*

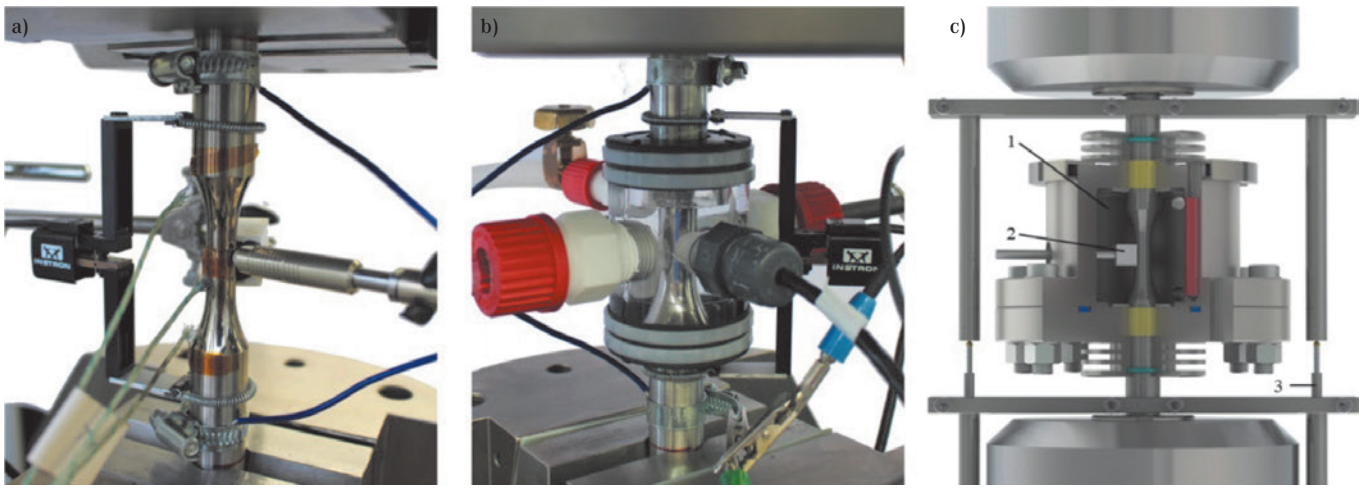


*Figure 3: Test setups for fatigue tests, a) in air, b) in distilled water, c) under reactor pressure vessel boiling water conditions in the autoclave*

uring the change in voltage in the gauge length of the specimen related to the microstructure from which the change in electrical resistance ΔR can be calculated. The electrical resistance depends on the specific electrical resistance ρ* which is a function of deformation induced microstructural changes.

The change in temperature ΔT of the specimen during the test was also measured [10]. For this purpose, three thermocouples were attached along the specimen. $T_1$ was located in the middle of the gauge length represented by the specimen's 10 mm minimum diameter and $T_2$ and $T_3$ were located on the shafts of the specimen having a diameter of 20 mm each. Due to the varied diameters, plastic deformations occur locally in the middle of the specimen representing the minimum cross-section. Subtracting the mean value of $T_2$ and $T_3$ from $T_1$, a difference in temperature ΔT can be calculated, which seems to result from the plastic deformation corrected for external influences (e. g. convection, thermal fluctuations) at the center of the gauge length. It may, therefore, be directly linked to the plastic strain amplitude $\varepsilon_{a,p}$. For other experiments at RT, an infrared camera with a spectral range of 7.5-13.0 µm, an optical resolution of 382 × 288 pixels and a thermal sensitivity of 40 mK was also used for temperature measurements, whereby the areas of measurement were defined in accordance with the procedure described above for the thermocouples, and the temperature information was processed equally.

Figure 3b shows an instrumented specimen for an experiment under medium conditions in distilled water. Preliminary tests on comparable metastable austenitic steels have shown no significant influence of the distilled water on the fatigue properties [11]. For these tests, the open circuit potential $E_{OCP}$ was measured, which provides additional information regarding the damage mechanisms occurring on the specimens' surface. During the measurement, the specimen itself serves as the working electrode. The reference electrode is a silver chloride electrode, and the counter electrode is made from graphite. Furthermore, electrical resistance measurements, as well as the self-developed magnetic field sensor, were applied.

For fatigue tests under reactor pressure vessel boiling water conditions (BWR), the tests were performed at 70 bar and 240 °C. High-temperature water with a conductivity of ~ 0.055 µS × cm$^{-1}$ was provided via a water treatment plant. Impurities by chloride ions were kept below 2 µg × kg$^{-1}$ and sulfate ions were generally well below 5 µg × kg$^{-1}$, which corresponds to the quality of the reactor water in BWR plants in normal operation according to VGB guidelines [12]. The oxygen content in the inlet was set to 400 µg × kg$^{-1}$ (0.4 ppm), which corresponds to the upper limit for BWR plants and is used in international investigations, mostly in laboratory tests to simulate BWR conditions.

The specially designed autoclave was adapted for the use of non-destructive measurement techniques, as shown in Figure 3c. High precision ceramic sleeves ensure the complete electrical insulation of the sample from the entire system. Thus, electrical resistance measurements can also be realized. Additionally, the electric circuit potential was measured using an external Ag/AgCl-electrode connected to a Teflon-coated asbestos filament which serves as an ion conductor. Thus, in the vicinity of the phase boundary metal-electrolyte (specimen–high temperature water), an equilibrium electric circuit potential can be measured. Basically, this electric circuit potential can be considered as a measure of the corrosion protection effect of the oxide layer and specifically describes the damage to the material induced by corrosion fatigue.

## Test results

**Tests at room temperature.** Figure 4a shows the results of a SIT in air at RT for AISI 347 in the initial condition with the course of the correlated total strain amplitude $\varepsilon_{a,t,cor}$, the stress amplitude $\sigma_a$, the change in temperature ΔT and the change in the tangential magnetic field $\Delta M_{tang}$. In all SITs performed, the $\varepsilon_{a,t,cor}$ started from $\varepsilon_{a,t,cor,start} = 0.5 \times 10^{-3}$ and after a step length of Δt = 1,800 s, $\varepsilon_{a,t,cor}$ was increased by $\Delta\varepsilon_{a,t,cor} = 0.5 \times 10^{-3}$ until specimen's failure. The measured variables recorded by the various sensors mentioned above, provide extensive information with regard to the $\varepsilon_{a,t,cor}$-M-relationship, which will be discussed in more detail later in the context of the S-N curve evaluation.

The increase of independent $\sigma_a$ progresses stepwise up to a strain level of $\varepsilon_{a,t,cor} = 2.5 \times 10^{-3}$, whereas from $\varepsilon_{a,t,cor} = 3.0 \times 10^{-3}$ onwards, $\sigma_a$ continually increases along each strain level. The increase in stress becomes more significant when moving to the next strain levels and slows down again from the strain level of $\varepsilon_{a,t,cor} = 5.0 \times 10^{-3}$ onwards. This characteristic cyclic hardening behavior of the AISI 347 at RT is due to the gradual deformation-induced martensitic phase transformation. Right near specimen failure, a significant drop in stiffness can be observed, which is the reason for a decrease in $\sigma_a$.

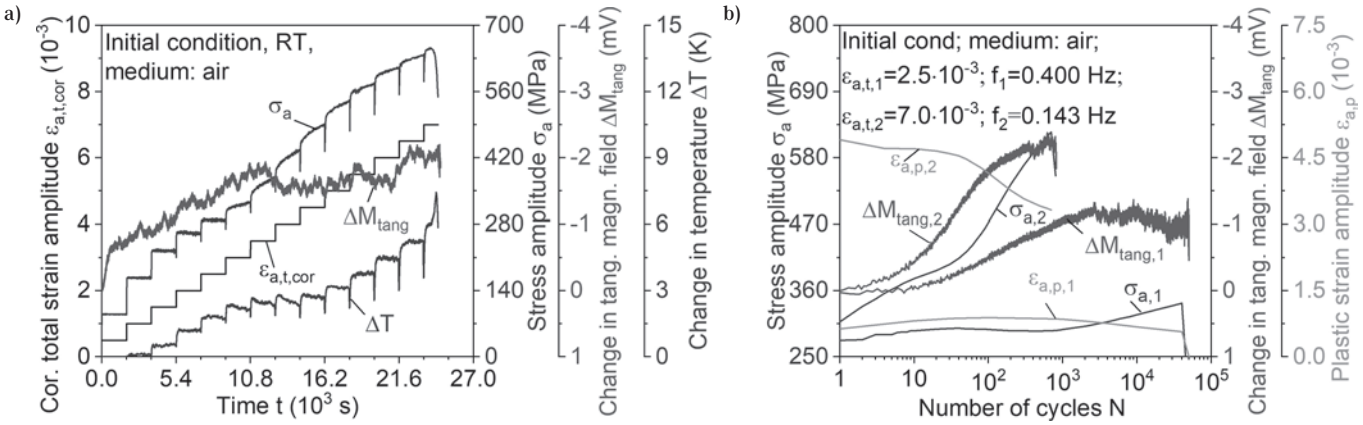


*Figure 4: a) Strain increase test, b) Constant amplitude tests in air for specimens in the initial state of AISI 347 (X6CrNiNb18-10)*

Furthermore, ΔT displays a behavior similar to $\sigma_a$ for the first 4 steps of the SIT. From $\varepsilon_{a,t,cor} = 2.5 \times 10^{-3}$ onwards, the ΔT signal slightly decreases within the steps which can be related to the cyclic hardening mechanisms during cyclic loading.

$\Delta M_{tang}$ shows a continuous increase up to $\varepsilon_{a,t,cor} = 3.5 \times 10^{-3}$ where at $\varepsilon_{a,t,cor} = 3.5 \times 10^{-3}$ a discontinuity in the slope is recognized. At $\varepsilon_{a,t,cor} = 3.5 \times 10^{-3}$, the slope decreases, which can be explained by the deformation induced martensitic phase transformation. From $\varepsilon_{a,t,cor} = 6.0 \times 10^{-3}$ onwards, a further change in $\Delta M_{tang}$ is observed which is probably due to macro-crack propagation occurring at this stage.

In order to use the StrainLife short time evaluation procedure (STEP), described in a subsequent section, two additional CATs (see Figure 4b) are required whose total strain amplitudes are selected based on the results of the SIT shown in Figure 4a. The development of the plastic strain amplitude $\varepsilon_{a,p}$ obtained from those CATs performed at strain amplitudes of $\varepsilon_{a,t,cor} = 2.5 \times 10^{-3}$ and $7.0 \times 10^{-3}$, respectively, and the curves for the $\sigma_a$ and $\Delta M_{tang}$ measurements taken during those tests are shown in Figure 4b. $\sigma_a$ and $\varepsilon_{a,p}$ show a stronger increase ($\sigma_a$) at 5-10 % of the constant amplitude fatigue life and decrease ($\varepsilon_{a,p}$), respectively, which can be related to the cyclic hardening behavior of the material. $\Delta M_{tang}$ rises continuously for both CATs at the beginning, followed by a saturation stage at ~ 40 % of the lifetime, which can again be related to the deformation-induced martensite formation. Further $\Delta M_{tang}$-value evolution is characterized by a continuous increase of those values until specimen failure.

**Tests under medium influence.** To compare the initial state with the defined aging state described before, SITs were carried out under distilled water medium conditions. Figure 5a shows results of a SIT with an AISI 347 specimen in the initial state, with the controlled value $\varepsilon_{a,t,cor}$, the stress amplitude $\sigma_a$, the open-circuit potential $E_{OCP}$ and the change in the tangential magnetic field $\Delta M_{tang}$ until specimen failure at $\varepsilon_{a,t,cor} = 9.5 \times 10^{-3}$, respectively. Until the strain level of $\varepsilon_{a,t,cor} = 3.5 \times 10^{-3}$ is reached, $\sigma_a$ also increases stepwise, whereas from $\varepsilon_{a,t,cor} = 4.0 \times 10^{-3}$ onwards, the $\sigma_a$ increase, depending on the stepwise increase of the total strain amplitude, is superimposed by an additional relative increase within each step. Just before specimen failure at $\varepsilon_{a,t,cor} = 9.5 \times 10^{-3}$, there is a significant drop in stiffness which is associated with a drop of $\sigma_a$. $E_{OCP}$ shows an almost constant behavior until $\varepsilon_{a,t,cor} = 3.5 \times 10^{-3}$. The course of $E_{OCP}$ slightly decreases from $\varepsilon_{a,t,cor} = 4.0 \times 10^{-3}$ onwards, also followed by an additional relative decrease within each loading step starting from $\varepsilon_{a,t,cor} = 8.5 \times 10^{-3}$ onwards. $\Delta M_{tang}$ stepwise decreases with increasing $\varepsilon_{a,t,cor}$, with an increasing gradient from $\varepsilon_{a,t,cor} = 2.0 \times 10^{-3}$ onwards. In the range $4.0 \times 10^{-3} < \varepsilon_{a,t,cor} < 7.0 \times 10^{-3}$, there is a relative increase within the steps caused by the martensitic phase transformation. Specimen failure is indicated in the step with $\varepsilon_{a,t,cor} = 9.5 \times 10^{-3}$ by a strong decrease in the $\Delta M_{tang}$ signal.

Figure 5b shows the SIT for the aged AISI 347. Due to the same testing procedure, the slopes of the aged and the unaged condition can be directly compared to each other. Specimen's failure occurs at the $\varepsilon_{a,t,cor} = 7.0 \times 10^{-3}$ strain level which is five strain levels below the unaged condition (see Figure 5a). $\sigma_a$ and $\Delta M_{tang}$ display qualitatively similar slopes when compared with the initial condition, with a first relative increase in $\sigma_a$ and a decrease in $\Delta M_{tang}$ within the step of $\varepsilon_{a,t,cor} = 4.0 \times 10^{-3}$, respectively. In contrast to that, $E_{OCP}$ shows a clearly distinguishable behavior. When compared to the unaged condition, $E_{OCP}$ of the aged specimen is stable until $\varepsilon_{a,t,cor} = 2.5 \times 10^{-3}$ followed by a decrease with larger relative decreases within the steps. For $\varepsilon_{a,t,cor} = 4.5 \times 10^{-3}$ and the following three stages, $E_{OCP}$ is almost constant within the confines of each step and decreases almost continuously from $\varepsilon_{a,t,cor} = 6.0 \times 10^{-3}$, where the fracture process then takes place.

In both SITs, the absolute increase of $\sigma_a$ in the first three stages is related to a purely elastic behavior, which can be broken down to a linear stress-strain relationship. From $\varepsilon_{a,t,cor} = 4.0 \times 10^{-3}$ onwards, for the initial state and $\varepsilon_{a,t,cor} = 4.5 \times 10^{-3}$ onwards, for the aged state, the increase in $\sigma_a$ is again dominated by the cyclic hardening process which is mostly related to the increase in dislocation density through the specimen's elongation during cyclic loading. Right before failure, $\sigma_a$ decreases in both cases, which is an indication for macrocrack initiation and propagation.

The course of $E_{OCP}$ provides additional information regarding the damage progress on the specimen's surface. Its constant course at the beginning of the test indicates that the specimens are electrochemically stabilized and that there are no active surfaces in the transition zone between the medium and the material. The following gradual descent proceeds with the change of $\varepsilon_{a,t,cor}$ or $\sigma_a$ and is based on the fact that as a result of slipping plane activities and the associated intrusions and extrusions, new active surfaces are exposed leading to a lowering in each stage of the $E_{OCP}$-level. If the hardening rate decreases (visible in $\sigma_a$), $E_{OCP}$ simultaneously starts to decrease stepwise. This is due to stable crack growth with continually newly exposed active surfaces until final unstable crack growth leads to a stronger drop of the values. In comparison, the constant range at the beginning of the test is shorter for the aged specimen, which can be attributed to the pre-damaging of the aging process. The partly distinctive relative changes in

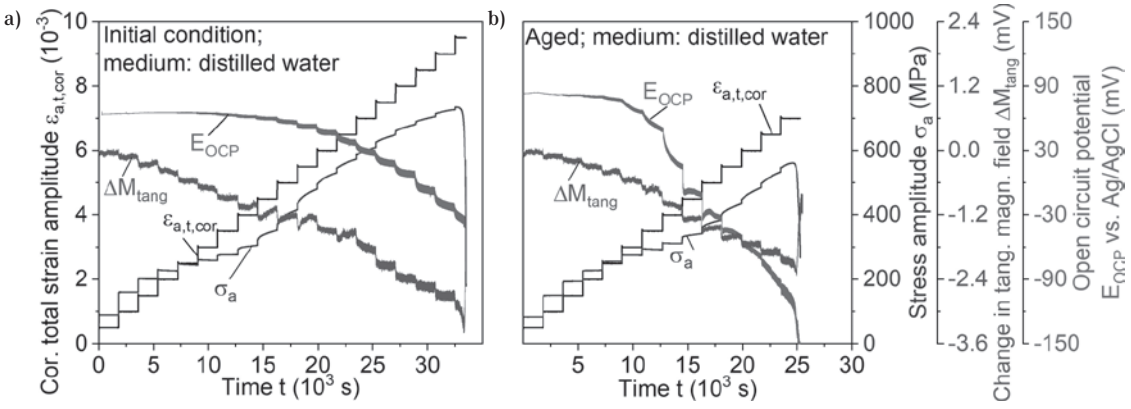


*Figure 5: Strain increase tests performed on AISI 347 (X6CrNiNb18-10) in distilled water for a) initial condition, b) aged condition*

the step transition are related to the fact that microcracks and associated material separation are already present in the material at this time, leading to anodic metal dissolutions. After macro crack initiation at $\varepsilon_{a,t,cor} = 5.5 \times 10^{-3}$, $E_{OCP}$ decreases continuously, which is due to stable crack growth followed by unstable crack growth in the last stage [13].

**Tests under reactor pressure vessel boiling water conditions.** Figure 6a shows the results of a SIT under BWR conditions at 240 °C and 70 bar for AISI 347 in the initial condition where the development of the total strain amplitude $\varepsilon_{a,t,cor}$, the plastic strain amplitude $\varepsilon_{a,p}$, the stress amplitude $\sigma_a$ and the absolute change in electric circuit potential $\Delta E_{CP}$ over the lifetime are shown, respectively. The parameters in this SIT are the same as described before for the test at RT. The strain level leading to the specimen's failure was $\varepsilon_{a,t,cor} = 8.5 \times 10^{-3}$, which is slightly lower than for the test in distilled water (see Figure 5a).

$\sigma_a$ initially increases stepwise up to a strain level of $\varepsilon_{a,t,cor} = 1.0 \times 10^{-3}$, whereas from $\varepsilon_{a,t,cor} = 1.5 \times 10^{-3}$ to $\varepsilon_{a,t,cor} = 3.0 \times 10^{-3}$ the individual $\sigma_a$ increase for these strain levels is superimposed by a continuous decrease in $\sigma_a$ within each step, related to the cyclic softening behavior of the material investigated. This behavior was not observed in tests at RT since at T = 240 °C there is no phase transformation from metastable austenite to martensite. From $\varepsilon_{a,t,cor} = 3.5 \times 10^{-3}$ onwards, the slope of $\sigma_a$ remains constant within each step. Approaching specimen failure, a significant drop in stiffness can be observed, which is seen as a decrease in $\sigma_a$. On the other hand, $\Delta E_{CP}$ displays stabilized behavior until $\varepsilon_{a,t,cor} = 3.0 \times 10^{-3}$. It has been shown in [14], that the oxide layer can already be damaged at total strain amplitudes of $1.8 \times 10^{-3}$. However, in this SIT, due to the reduced length of each step, this effect is first visible at $\varepsilon_{a,t,cor} = 3.0 \times 10^{-3}$. Between $\varepsilon_{a,t,cor} = 3.5 \times 10^{-3}$ and $5.0 \times 10^{-3}$ there is a slight increase in the absolute $\Delta E_{CP}$ value due to new active surfaces. From $\varepsilon_{a,t,cor} = 5.5 \times 10^{-3}$ onwards the increase in the value of $\Delta E_{CP}$ is more pronounced. In order to be used for the StrainLife STEP and a resulting S-N curve, two total strain controlled CATs (see Figure 6b) were performed at $\varepsilon_{a,t,cor} = 3.0 \times 10^{-3}$ and $5.5 \times 10^{-3}$, respectively. Figure 6b shows the courses of $\sigma_a$, $\Delta E_{CP}$ and $\varepsilon_{a,p}$, respectively. For the CAT with $\varepsilon_{a,t,cor} = 5.5 \times 10^{-3}$, $\sigma_a$ is characterized by a slight but continuous cyclic hardening followed by a decrease in stiffness just before specimen failure, whereas for the CAT with $\varepsilon_{a,t,cor} = 3.0 \times 10^{-3}$, $\sigma_a$ increases within the first 40 cycles until a local hardening maximum is reached, which is followed again by a slight decrease, being more pronounced during the last cycles before specimen failure. The $\Delta E_{CP}$ values remain stable until 10 to 15 % of the fatigue life, where first intrusions and extrusions start. It continues increasing for both CATs as new exposed active surfaces appear on the specimen until the fracture is finally achieved.

## S-N curve calculation and modeling

**StrainLife.** StrainLife is a newly developed STEP for the evaluation of S-N curves and is considered here for adaptation and validation in nuclear engineering applications. The value of STEPs can be seen in the fact

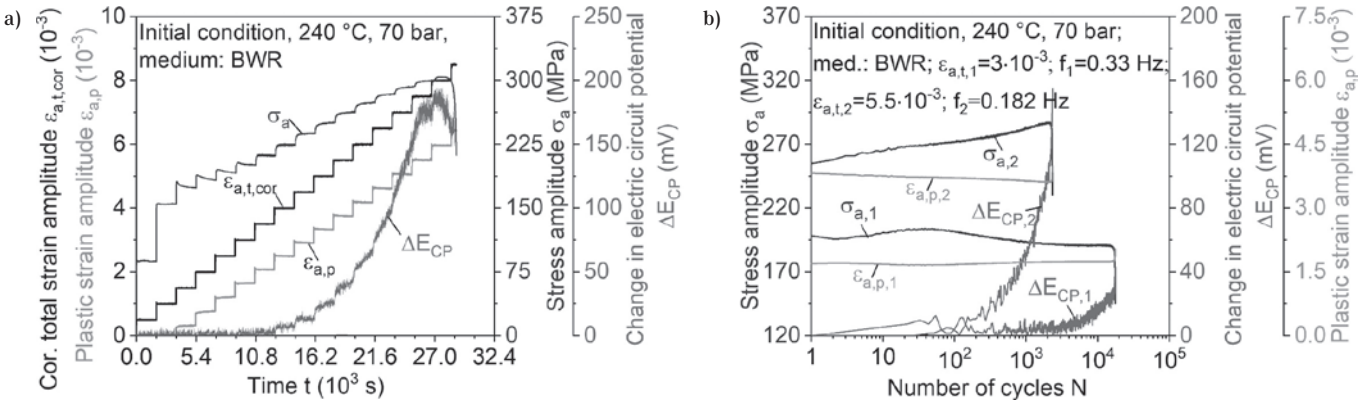


*Figure 6: Results for AISI 347 (X6CrNiNb18-10) in the initial state under BWR condition, a) strain increase test, b) constant amplitude tests*

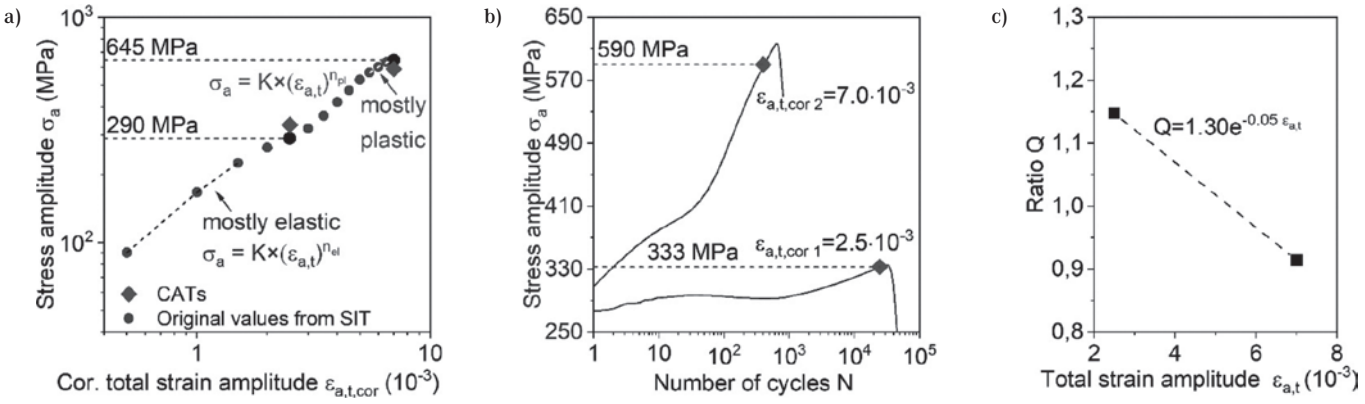


*Figure 7: a) Morrow curve for the SIT and the values of the stress amplitude at $N_f/2$ of the two CATs, b) cyclic deformation curves based on the stress amplitude for the two CATs with marked stress amplitude values at $N_f/2$, c) relationship of ratio Q vs. total strain amplitude for AISI 347 (X6CrNiNb18-10)*

that usually only one SIT and two total strain-controlled CATs are required for the evaluation of a complete total strain S-N curve. This is also the case in StrainLife, thus offering a significant advantage when compared to the conventional way of determining an equivalent S-N curve. The input variables for the StrainLife method are the measurands $\sigma_a$, $\varepsilon_{a,p}$, $\Delta T$, $E_{OCP}$, $\Delta M_{tang}$ and $\Delta E_{CP}$, respectively and their progressions over fatigue life as shown in various experiments presented above. The procedure is described below using the data presented in Figure 4 for $\sigma_a$-$\varepsilon_{a,e/p}$-value pairs, but can be transferred to the other measurands as well with respect to the comparable quality of the calculated results [11]. For the calculation based on StrainLife, $\varepsilon_{a,t}$ is plotted vs. $\sigma_a$ in a Morrow [15] curve (see Figure 7a) in which a predominantly elastic (el) and predominantly plastic (pl) region can be identified and mathematically described independently of each other with Equations (1) and (2).

$$\sigma_a = K_{el}' \cdot \left(\varepsilon_{a,t}\right)^{n_{el}'} \quad (1)$$

$$\sigma_a = K_{pl}' \cdot \left(\varepsilon_{a,t}\right)^{n_{pl}'} \quad (2)$$

with $K_{el}$' and $K_{pl}$': cyclic hardening coefficients and $n_{el}$' and $n_{pl}$': cyclic hardening exponents for the elastic and plastic region, respectively.

However, if the corresponding stabilized stress values at a defined reference point within the lifespan of the specimen (e. g. $\sigma_a$ for 0.5 × $N_f$) for the two CATs (see Figure 7b) are plotted in the same graph as the SIT (see Figure 7a), a small difference between the CAT and SIT values can be observed, which in this case is apparent in the predominantly plastic region. This is due to the fact that in each of the loading levels damage is generated in the SIT and the data pairs are extracted at different junctures in their lifespan. Hence, different portions of damage, as well as degrees of cyclic hardening, are attributed to the individual tests. To correct this, a ratio Q between the stress amplitude of the CAT and the SIT is calculated according to Equation (3).

$$Q = \frac{\sigma_a\left(CAT\right)}{\sigma_a\left(SIT\right)} \quad (3)$$

Using the calculated Q values for both strain levels, a fitting curve for the further extrapolation of the data can be calculated, where an exponential fit has been chosen, as shown in Figure 7c. By using this relationship, the stress-strain behavior of the SIT is transferred to the stress-strain behavior for the strain-controlled CATs (see Figure 8a).

Using Equations (1) and (2) and the distinction between the elastic range and the corrected plastic range, the fatigue strength exponent b (el) and fatigue ductility exponent c (pl) can be calculated using Equations (4) and (5), respectively.

$$b = \frac{-n_{el}'}{5n_{el}'+1} \quad (4)$$

$$c = \frac{-1}{5n_{pl}'+1} \quad (5)$$

The total strain amplitude $\varepsilon_{a,t}$ contains an elastic portion $\varepsilon_{a,e}$ and a plastic portion $\varepsilon_{a,p}$ (Equation (6)), which can be mathematically described by the Basquin (Equation (7)) [16] and Manson-Coffin equations (Equation (8)) [17] as functions of the number of cycles to failure.

$$\varepsilon_{a,t} = \varepsilon_{a,e} + \varepsilon_{a,p} \quad (6)$$

For total strain controlled SIT and CATs, the controlled value is $\varepsilon_{a,t}$, the plastic strain amplitude $\varepsilon_{a,p}$ is calculated for each cycle from the stress-strain hysteresis loop as its half-width and the elastic strain amplitude $\varepsilon_{a,p}$ is subsequently calculated using Equation (6).

By using the strain values of the CATs (e. g. $\varepsilon_{a,e}$ or $\varepsilon_{a,p}$ at 0.5 × $N_f$) from Figure 4b, the coefficients B and C can be calculated for $\varepsilon_{a,t,cor}$ = 2.5 × $10^{-3}$ and $\varepsilon_{a,t,cor}$ = 7.0 × $10^{-3}$, respectively.

$$\varepsilon_{a,e} = B \cdot \left(2N_f\right)^b \rightarrow B = \frac{\varepsilon_{a,e}}{(2N_f)^b} \quad (7)$$

$$\varepsilon_{a,p} = C \cdot \left(2N_f\right)^c \rightarrow C = \frac{\varepsilon_{a,p}}{(2N_f)^c} \quad (8)$$

If Equations (4) and (5) are used within Equations (7) and (8), Equation (9) is obtained, whereby not only the total strain S-N curve but also the portions of the Basquin (elastic) and Manson-Coffin (plastic) equations shown in Figure 8b can be determined.

$$\varepsilon_{a,t} = B \cdot \left(2N_f\right)^{\frac{-n_{el}'}{5n_{el}'+1}} + C \cdot \left(2N_f\right)^{\frac{-1}{5n_{pl}'+1}} \quad (9)$$

Figure 8b shows the evaluated total strain S-N curve according to the StrainLife method compared to 14 CATs, which were performed in accordance with a step-down procedure. In current investigations, the database is being comprehensively expanded for the purpose of validating the StrainLife method.

Since two CATs are used for the evaluation in addition to the SIT, two total strain S-N curves are obtained, as shown in Figure 9 for a calculation with $\varepsilon_{a,t,cor}$ = 2.5 × $10^{-3}$

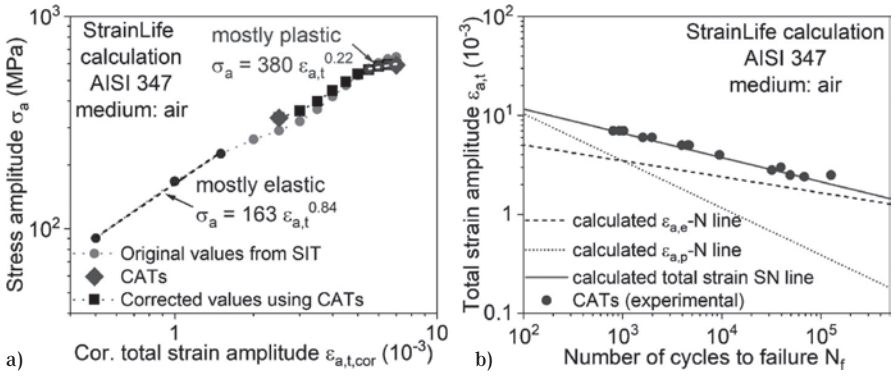


*Figure 8: a) Calculated Morrow curve with identified predominantly elastic and predominantly plastic regions, b) Comparison of the total strain*

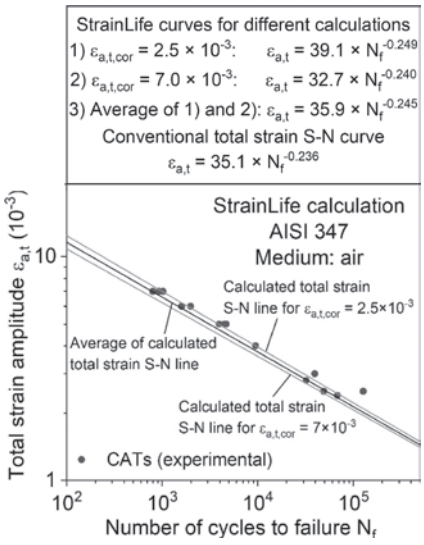


*Figure 9: Comparison of the total strain S-N curve determined through StrainLife for different total strain amplitudes with conventional determined total strain S-N data for the initial state of AISI 347 (X6CrNiNb18-10)*

and $\varepsilon_{a,t,cor} = 7.0 \times 10^{-3}$, respectively. In order to minimize the deviation from a conventionally determined S-N curve, these curves are averaged. The more CATs performed and included in the StrainLife calculation, the higher the assurance that the result is in accordance with conventionally determined S-N curves.

The same procedure described above can be used to evaluate S-N curves using other input parameters [18]. In Figure 10, the results of the StrainLife calculation are presented for the tests performed under BWR conditions (cf. Figure 6) by using the $\Delta E_{CP}$-$\varepsilon_{a,e/p}$ values. It can be seen that StrainLife as a STEP has significant potential for evaluating appropriate S-N curves even under BWR conditions and requiring only a fraction of experimental effort and cost.

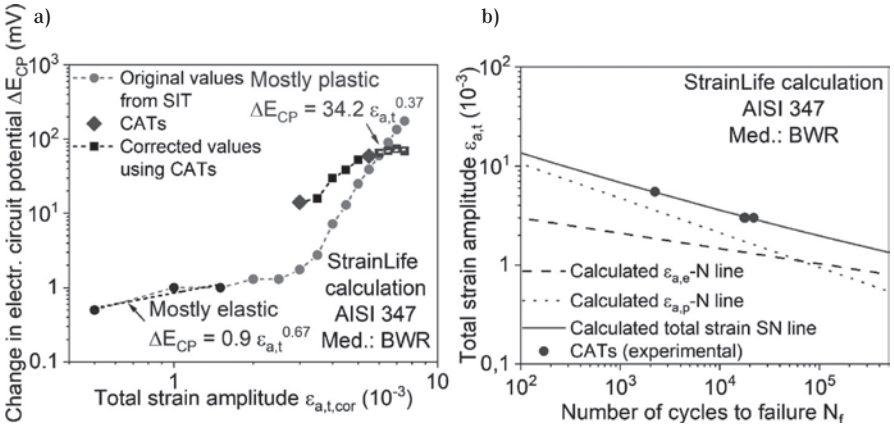


*Figure 10: a) Calculated Morrow curve for the electric circuit potential, b) Comparison of the StrainLife evaluated total strain S-N curve with conventionally determined independent S-N data for the initial state of AISI 347 (X6CrNiNb18-10) tested under BWR*

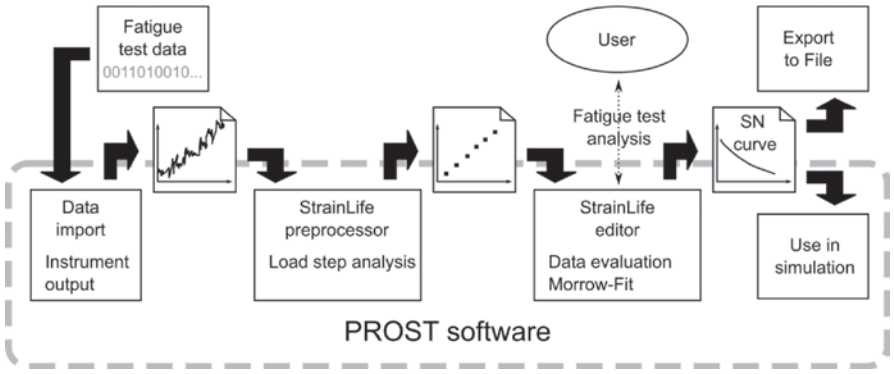


*Figure 11: StrainLife editor within PROST software*

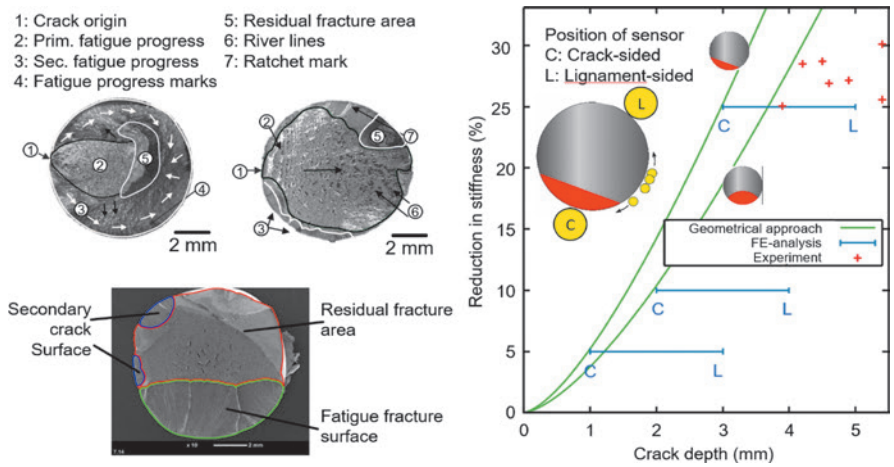


*Figure 12: Fractographic investigations and elastic-plastic finite element evaluation for AISI 347 (X6CrNiNb18-10)*

**Implementation of StrainLife into PROST.** The simulation program PROST [4] is a tool for the integrity assessment of pressurized components under operational or accidental loading conditions. It is suitable for the evaluation of cracks, for the determination of leak and break probabilities in pipelines and vessels and for the quantification of the various influencing variables related to component behavior. The code evaluates the behavior of an intact component, the transition to crack formation, crack initiation, and crack growth to leakage and fracture. The influence of recurring inspections and pressure tests as well as leak monitoring systems can also be considered in such simulations. Optionally, deterministic or probabilistic calculations are possible. While fracture mechanics parameters and crack growth laws corresponding to the material and damage mechanisms are assumed for the evaluation of crack growth, determination of the crack formation is based on S-N curves followed by assumptions on the initial crack size.

Through the StrainLife method, it is possible to process the NDT measurements along SITs and CATs and to get those converted to variables in the sense of a service or fatigue life evaluation. With respect to automation and a user-friendly application, StrainLife and other already established STEPs for the evaluation of S-N curves such as PHYBAL [19] have been developed as calculation routines and editors equipped with a graphical user interface implemented into PROST as parts of this structural-mechanical code. The workflow for the StrainLife implementation is shown in Figure 11.

The StrainLife editor takes the results of the SITs and CATs as input values. In the next step, the parameters for the evaluation routine are entered, for example, the definition of the predominantly elastic and predominantly plastic ranges of the material response, the determination of the coefficients B and C (Equations (7) and (8)) and a display of the intermediate result as plain text in the output window. The resulting total strain S-N curve, the curves based on the Morrow equation and the M–$N_f$ correlations of the CATs can be displayed in PROST, applied in assessment simulations and exported for use in other tools.

**Crack size simulation.** In order to derive information regarding crack size from

the load drop, a finite element half model for fatigue tests with unnotched specimens of AISI 347 was designed. Secant cracks (as shown in Figure 12) of varied depths were assumed. Here the azimuthal position of the extensometer used for mechanical strain measurements relative to the crack is important. If the extensometer is mounted on the side where crack formation occurs (C), the crack size for a given load drop is smaller than when the extensometer is mounted at the opposite ligament side (L).

To determine the correlation between load drop and crack size, elastic-plastic finite element calculations were performed with consideration of the different sensor positions. This results in a value range of crack depths for different load drops. In the case of a 25 % load drop, possible crack depths between 3 and 5 mm are obtained. First test results of specimens broken apart after reaching the defined load drops confirm certain crack geometry assumptions.

## Conclusions

This article shows that non-destructive and electrochemical measurement methods can be used to derive parameters which can be used for an improved evaluation of the fatigue damage behavior of aging austenitic metallic materials used in nuclear engineering such as metastable AISI 347 (X6CrNiNb18-10). Temperature, electric resistance, tangential magnetic field or a change in electric circuit potential are among those non-destructive testing (NDT) based parameters which show adequate if not better performance compared with plastic strain amplitude which is one of the state-of-the-art parameters and measurement techniques. Parameters derived from those NDT techniques can possibly be more easily accessed when compared to plastic strain measurement, and they may possibly be more sensitive when looking at specific cases where this article only provides a limited example and can still not claim to demonstrate the full potential of this approach.

It has been shown that in the case of distilled water and boiling water reactor medium conditions, NDT measures still hold and that the NDT parameters can even be derived appropriately under such environmental conditions. Since the NDT based parameters derived can be used to determine S-N curves by means of short time evaluation procedures (STEP), where only a fraction of effort is required to generate an S-N curve when compared to state-of-the-art, a completely new field of generating S-N data has been opened. In light of the fact that the components in nuclear engineering are often exposed to strain controlled loading, at least in those locations where fatigue damage becomes critical, the StrainLife method has been specifically developed as a STEP and explained here. It would be advantageous for such a method to become an integral part of structure mechanical analysis codes in nuclear engineering areas where PROST which has been briefly described is applied. Implementing such methods in tools for integrity assessment does not only ease the provision and application of S-N data within the code but can also help to guide the inspection processes of components in the future so that the code may be able to predict which parameter would be measured best at which location and how accumulated damage may be assessed best at a macroscopically still uncracked stage. Proof for such an idea will be considered as a next step within the MibaLeb project phase II.

## Acknowledgment

Work presented in this article has been carried out within the framework of the joint project “Microstructure-based determination of the maximum service life for corrosion fatigue loaded materials and components of nuclear technology” funded by the Federal Ministry of Economics and Energy (BMWi) coded 1501528A, 1501528B, 1501528C and RS1545 respectively.

## References

1 Kompetenzverbund Kerntechnik: Nukleare Sicherheitsforschung – Neuorientierung an aktuellen energiepolitischen Rahmenbedingungen, GRS, Cologne, Germany (2013)
2 G. Dobmann, C. Boller, H. G. Herrmann, I. Altpeter: Electromagnetic NDT for lifetime management by monitoring of ageing phenomena, Proc. of the 12th International Conference of the Slovenian Society for Nondestructive Testing, Portorož, Slovenia (2013), pp. 293-302
3 K. Heckmann, H. Grebner, J. Sievers: Further development of probabilistic analysis method for lifetime determination of piping and Vessels (Weiterentwicklung probabilistischer Analysemethoden zur Lebensdauerbestimmung von Rohrleitungen und Behältern), GRS – A – 3709, Final report Reactor Safety Research – Project No.: RS1196, Germany (2013)
4 K. Heckmann, J. Sievers: Code development for piping integrity assessment with respect to new German safety standard, Proc. of the 23rd International Conference on Structural Mechanics in Reactor Technology (SMiRT 23), Manchester, United Kingdom (2015), pp. 916-925
5 A. Sorich, M. Smaga, D. Eifler: Estimation of the fatigue limit due to cyclic hardening and softening processes, Subproject: Experimental investigations (Bewertung der Ermüdungsfestigkeit unter Berücksichtigung zyklischer Ver- und Entfestigungsvorgänge, Teilprojekt: Experimentelle Untersuchungen), Final report Reactor Safety Research – Project No.: 1501395B, Germany (2014)
6 H. Waidele, T. Weißenberg: Zentrale Untersuchung und Auswertung von Herstellungsfehlern und Betriebsschäden im Hinblick auf druckführende Anlagenteile von Kernkraftwerken, Arbeitspaket 3, Einfluss des Reaktorkühlmediums auf das Ermüdungsverhalten austenitischer Rohrleitungen, BMU-Vorhaben SR 2501, MPA Universität Stuttgart, Germany (2007)
7 O. Chopra, G. L. Stevens: Effect of LWR Water Environments on the Fatigue Life of Reactor Materials (NUREG/CR–6909, Revision 1) – Final Report, United States Nuclear Regulatory Commission, United States (2018)
8 M. Smaga, R. Skorupski, P. Mayer, B. Kirsch, J. C. Aurich, I. Raid, J. Seewig, J. Man, D. Eifler, T. Beck: Influence of surface morphology on fatigue behavior of metastable austenitic stainless steel AISI 347 at ambient temperature and 300 °C, Procedia Structural Integrity 5 (2017), pp. 989-996 DOI:10.1016/j.prostr.2017.07.150
9 P. Starke, F. Walther, D. Eifler: Model-based correlation between change of electrical resistance and change of dislocation density of fatigued-loaded ICE R7 wheel steel specimens, Materials Testing 60 (2018), No. 7-8, pp. 669-677 DOI:10.3139/120.111202
10 H. Knobbe, P. Starke, S. Hereñu, H. J. Christ, D. Eifler: Cyclic deformation behaviour, microstructural evolution and fatigue life of duplex steel AISI 329 LN, International Journal of Fatigue 80 (2015), No. 5, pp. 81-89 DOI:10.1016/j.ijfatigue.2015.05.002
11 M. Klein, P. Starke, D. Nowak, C. Boller, F. Walther: Separation of surface, subsurface and volume fatigue damage effects in AISI 348 steel for power plant applications, Materials Testing 58 (2016), No. 7-8, pp. 601-607 DOI:10.3139/120.110896
12 M. Rosskamp, N. Albrecht, U. Ilg, H. Neder, U. Reitzner, B. Riedmueller, D. Rutschow: VGB guideline for the water in nuclear power plants with light water reactors (BWR) VGB-R 401 J, VGB PowerTech 87 (2007), No. 3, pp. 73-79
13 F. Maci, M. Jamrozy, R. Acosta, P. Starke, C. Boller, K. Heckmann, J. Sievers, T. Schopf, F. Walther: Characterization of the fatigue behavior of mechanical and thermal aged austenitic power plant steel AISI 347. In: J. Correia, A. De Jesus, A. Fernandes, R. Calçada (eds.): Mechanical Fatigue of Metals, Structural Integrity 7, Springer Nature Switzerland AG (2019), pp. 65-71 DOI:10.1007/978-3-030-13980-3_9
14 H. Kanasaki, R. Umehara, H. Mizuta, T. Suyama: Effects of strain rate and temperature change on the fatigue life of stainless steel in PWR primary water, 14th International Conference on Structural Mechanics in Reactor Technology (SMiRT 14), Lyon, France (1997), pp. 487-493

15 J. Morrow: Cyclic plastic strain energy and fatigue of metals, Internal Friction, Damping, and Cyclic Plasticity, American Society for Testing and Materials 10 (1965), pp. 45-87 DOI:10.1520/STP43764S
16 O. H. Basquin: The exponential law on endurance tests, American Society for Testing and Materials 10 (1910), pp. 625-630
17 S. S. Manson: Fatigue: A complex subject – Some simple approximations, Experimental Mechanics 5 (1965), No. 4, pp. 193-226 DOI:10.1007/BF02321056
18 P. Starke, D. Eifler, C. Boller: Fatigue Assessment of Metallic Materials beyond Strain Measurement, International Journal of Fatigue 82 (2016), pp. 274-279 DOI:10.1016/j.ijfatigue.2015.03.018
19 P. Starke, F. Walther, D. Eifler: New fatigue life calculation method for quenched and tempered steel SAE 4140, Materials Science and Engineering A 523 (2009), No. 1-2, pp. 246-252 DOI:10.1016/j.msea.2009.05.067

## Bibliography

DOI 10.3139/120.111417
Materials Testing
61 (2019) 11, pages 1029-1038

ISSN 0025-5300

## The authors of this contribution

MSc Ruth Acosta, born in 1988, studied Civil Engineering at José Simeón Cañas Central American University (UCA), El Salvador and received a Master of Sciences in Non-Destructive Testing at Dresden International University, Germany. Since 2017, she has been working as a research associate at the Chair of Non-Destructive Testing and Quality Assurance at Saarland University and since 2018, she has also been working as a Research Associate at the University of Applied Sciences Kaiserslautern (Hochschule Kaiserslautern) in Germany. Her research is mainly focused on the use of non-destructive methods for the characterization and detection of defects in metallic materials.

Prof. Dr.-Ing. Christian Boller, born in 1954, graduated from the Technische Hochschule (now Technische Universität) Darmstadt/Germany in Structural Engineering (Civil Engineering) in 1980 and received a Doctoral degree from the same institution in Materials Mechanics in 1987. Thereafter, he worked at institutions like Battelle, Daimler and MBB (today Airbus) where he became Chief Engineer for Structures in the military aircraft division. In 2003 he was appointed a full professor in Smart Structural Design at the University of Sheffield/UK and assumed the chair for NDT and quality assurance at Saarland University in 2008, which he still maintains. He has published more than 300 scientific papers, reports and books and has been Scientific Director of the NDT master course at Dresden Internat. Univ. since 2013. Moreover, he has been a visiting professor at the Nanjing University of Aeronautics and Astronautics (NUAA) in Nanjing/China since 2014 and a member of various editorial and scientific boards.

Prof. Dr.-Ing. Peter Starke, born in 1977, studied Mechanical Engineering at the TU Kaiserslautern, Germany. In 2002 he became a research assistant at the Institute of Materials Science and Engineering (WKK) at TU Kaiserslautern, Germany. He received his engineering doctoral degree in 2007 writing on "The fatigue life calculation of metallic materials under constant amplitude loading and service loading". From 2007 to 2012 he headed the research group "Fatigue life calculation" at WKK. Afterwards, he changed to Fraunhofer IZFP in Saarbrücken, Germany. From 2013 to 2018 he was in the position of a Senior Research Associate at the Chair of Non-Destructive Testing and Quality Assurance at Saarland University in Saarbrücken, Germany. In 2018 he became a Professor in the field of Materials Science and Materials Testing at the University of Applied Sciences Kaiserslautern (Hochschule Kaiserslautern). His research is mainly focused on the use of non-destructive measurement techniques for the characterization of the fatigue behavior and the fatigue life calculation of metallic and non-metallic materials in the LCF-, HCF- and VHCF-regime as well as for the evaluation of defects and inhomogeneities in the material's microstructure.

MSc Michael Jamrozy, born in 1992, studied Mechanical Engineering with a focus on Materials Science at the TU Dortmund University, Germany where he received his Master degree in 2017. He worked as a Student Assistant in the Department of Materials Test Engineering (WPT) at the TU Dortmund University from 2014 to 2017 in the field of fiber-reinforced polymers. Since 2017 he has been working as a scientific assistant at the WPT with a research focus on the orientation-dependent material behavior of wood-based materials.

Dr.-Ing. Marina Knyazeva, born in 1979, studied Materials Science at Altai State Technical University, Russia. After her diploma thesis, she worked as Scientific Assistant at the Chair for Technology of Composite Materials at the same university and continued her career at the Chair of Materials Testing at the Ruhr-University Bochum, Germany. There she received her PhD in Mechanical Engineering in 2015. Currently she is a Postdoctoral Researcher in the Department of Materials Test Engineering at the TU Dortmund University, Germany. Her main research interests are the microscopic, mechanical and technological characterization of material behavior with the special focus on impact of environmental conditions.

Prof. Dr.-Ing. Frank Walther, born in 1970, studied Mechanical Engineering majoring in Materials Science and Engineering at TU Kaiserslautern University, Germany. There he finished his PhD on the fatigue assessment of railway wheel steels in 2002 and his habilitation on physical measurement techniques for microstructural-based fatigue assessment and lifetime calculation of metals in 2007. At Schaeffler AG in Herzogenaurach, Germany, he took responsibility for Public Private Partnership within Corporate Development from 2008 to 2010. Since 2010 he has been Professor for Materials Test Engineering (WPT) at the TU Dortmund University, Germany. His research portfolio includes determination of process-structure-property-damage relationships of metal- and polymer-based materials and components under fatigue loading from LCF to VHCF range, taking the influence of manufacturing and joining processes as well as service loading and corrosion deterioration into account.

Dr. rer. nat. Klaus Heckmann, born in 1982, studied Physics at TU Darmstadt and INP Grenoble, and obtained his PhD in Darmstadt with a thesis on transport properties of hot and dense matter. Since 2012, he has been working at GRS in Cologne, Germany, as a Technical Expert for structural mechanics. His field of research comprises the safety assessment of metallic components, the description of aging processes and computational simulation, especially for piping components. He is currently responsible for the development project of GRS' structure simulation software PROST.

Dr. rer. nat. habil. Jürgen Sievers, born in 1955, studied Physics at the University of Cologne and received his PhD in 1983. He attained post-doctoral lecture qualifications at the University of Stuttgart in 2002. Since 1982 he has been working at GRS and contributes to research projects on the deterministic integrity assessment of metallic components and concrete structures under loads due to design basis accidents up to severe accidents, fracture assessment of cracks, leak-before-break analysis including leak rate calculation and structure mechanical issues in probabilistic safety analysis. He is Chief Expert in the field of computational structure mechanics and Project Manager of nuclear research projects on analysis methods for integrity assessment of components and structures. He is author/coauthor of more than 200 technical papers and reports in the area of structural mechanics, fracture mechanics, integrity of metallic and concrete components as well as interdisciplinary aspects. As a member of the Project Committee on "Component Integrity" he has been supporting the Project Management Agency of the Reactor Safety Research Program financed by the Federal Ministry of Economics and Technology (BMWi) concerning evaluation of research projects since 2006. He was co-ordinator of the international research projects FALSIRE, RPV PTS ICAS and COSSAL sponsored by OECD/NEA. Since 2012 he has been Chairman of the CSNI Working Group on Integrity and Aging of Components and Structures (WGIAGE).

MSc Tim Schopf, born in 1989, studied Mechanical Engineering at Stuttgart University, majoring in Materials Testing and Strength of Materials. Since 2017, he has been working as a Research Associate at the Materials Testing Institute, University of Stuttgart, Germany. His research is mainly focused on the fatigue behavior of austenitic steels and relevant filler metals under boiling water reactor medium conditions. He also works on numerical methods and analysis to assess fatigue behavior in the high cycle fatigue and very high cycle fatigue regime.

Prof. Dr. Stefan Weihe is Director of the Materials Testing Institute (MPA) as well as being Head and Full Professor at the Institute of Materials Testing, Materials Science and Strength of Materials (IMWF), University of Stuttgart, Germany, since 08/2014. He received his doctorate in Aerospace Engineering at the Institute for Statics and Dynamics of Aerospace Structures, University of Stuttgart in 1998 and before working as a Senior Expert for Chassis Strength, Friction and Wear for Audi AG, Ingolstadt, Germany. From 2002 to 2014 he was a Senior Manager in the field of Strength and Fatigue, Body in White, and Body Concepts and Advanced Engineering in the Development & Research Department, Division Mercedes-Benz Vans, Daimler AG, Stuttgart, Germany.